Structure of an Active Soluble Mutant of the Membrane-Associated (*S*)-Mandelate Dehydrogenase[†,‡]

Narayanasami Sukumar,[§,||] Yang Xu,[||,⊥] Domenico L. Gatti,[⊥] Bharati Mitra,[⊥] and F. Scott Mathews*[,§]

Department of Biochemistry and Molecular Biophysics, Washington University School of Medicine, St. Louis, Missouri 63110, and Department of Biochemistry and Molecular Biology, School of Medicine, Wayne State University, Detroit, Michigan 48201

Received May 8, 2001; Revised Manuscript Received June 7, 2001

ABSTRACT: The structure of an active mutant of (*S*)-mandelate dehydrogenase (MDH-GOX2) from *Pseudomonas putida* has been determined at 2.15 Å resolution. The membrane-associated flavoenzyme (*S*)-mandelate dehydrogenase (MDH) catalyzes the oxidation of (*S*)-mandelate to give a flavin hydroquinone intermediate which is subsequently reoxidized by an organic oxidant residing in the membrane. The enzyme was rendered soluble by replacing its 39-residue membrane-binding peptide segment with a corresponding 20-residue segment from its soluble homologue, glycolate oxidase (GOX). Because of their amphipathic nature and peculiar solubilization properties, membrane proteins are notoriously difficult to crystallize, yet represent a large fraction of the proteins encoded by genomes currently being deciphered. Here we present the first report of such a structure in which an internal membrane-binding segment has been replaced, leading to successful crystallization of the fully active enzyme in the absence of detergents. This approach may have general application to other membrane-bound proteins. The overall fold of the molecule is that of a TIM barrel, and it forms a tight tetramer within the crystal lattice that has circular 4-fold symmetry. The structure of MDH-GOX2 reveals how this molecule can interact with a membrane, although it is limited by the absence of a membrane-binding segment. MDH-GOX2 and GOX adopt similar conformations, yet they retain features characteristic of membrane and globular proteins, respectively. MDH-GOX2 has a distinctly electropositive surface capable of interacting with the membrane, while the opposite surface is largely electronegative. GOX shows no such pattern. MDH appears to form a new class of monotopic integral membrane protein that interacts with the membrane through coplanar electrostatic binding surfaces and hydrophobic interactions, thus combining features of both the prostaglandin synthase/squaline-hopine cyclase and the C-2 coagulation factor domain classes of membrane proteins.

(*S*)-Mandelate dehydrogenase (MDH)[1] from *Pseudomonas putida* oxidizes (*S*)-mandelate to phenylglyoxalate. It is an enzyme in the mandelate pathway that occurs in several strains of *Pseudomonas* which converts (*R*)-mandelate to benzoate (*1*). MDH is a member of a widespread family of homologous FMN-dependent α-hydroxyacid oxidizing enzymes. This family occurs in both prokaryotes and eukaryotes, including archaebacteria, *Pseudomonads*, yeasts, plants, and mammals. In addition to MDH, members of this family include flavocytochrome b_2 (FCB2, yeast), glycolate oxidase (GOX, spinach), lactate monooxygenase (LMO, bacteria), and long chain hydroxyacid oxidase (LCHAO, mammals). Together, they share a common active site arrangement (*2*) and sequence motif (*3*), ∼30−45% amino acid sequence identity existing between individual family members. The best biochemically characterized of these enzymes are FCB2 (*4*) and LMO (*5*), whereas crystallographic studies have focused on FCB2 and GOX to the greatest extent (*6*−*8*).

All of the enzymes follow a ping-pong mechanism in which the α-hydroxyacid substrate is first oxidized by the enzyme to form the product and the flavin is reduced to the hydroquinone (the reductive half-reaction). In a second step (the oxidative half-reaction), the reduced flavin is reoxidized by an electron acceptor. The reductive half-reaction appears to follow a common reaction mechanism within the family involving either substrate α-proton abstraction to form a carbanion intermediate or the direct transfer of a hydride from the substrate α-carbon to the flavin ring (*9*). The oxidative half-reaction differs among the enzymes. For GOX, LCHAO, and LMO, the electron acceptor from the flavin is molecular oxygen, which leads to formation of hydrogen peroxide (GOX and LCHAO) or hydroxylated product (LMO). For FCB2, the external electron acceptor is cytochrome *c*, to which electron transfer is mediated by a *b*-type cytochrome domain within the enzyme. In MDH, the electron acceptor is a component of the electron transfer chain within the bacterial membrane, possibly a quinone.

[†] This work has been supported in part by U.S. Public Health Service Grant 20530 (F.S.M.) and by U.S. Public Health Service Grant 54102 (B.M.).

[‡] Crystallographic coordinates have been deposited in the Protein Data Bank as entry 1HUV.

* To whom correspondence should be addressed. E-mail: mathews@biochem.wustl.edu. Telephone: (314) 362-1080. Fax: (314) 362-7183.

[§] Washington University School of Medicine.

[||] These authors contributed equally to this work.

[⊥] Wayne State University.

[1] Abbreviations: MDH, (*S*)-mandelate dehydrogenase; MDH-GOX2, chimeric mutant of (*S*)-mandelate dehydrogenase with residues 177−215 replaced with residues 176−195 of glycolate oxidase; GOX, glycolate oxidase from spinach.

10.1021/bi010938k CCC: $20.00
Published on Web 07/26/2001

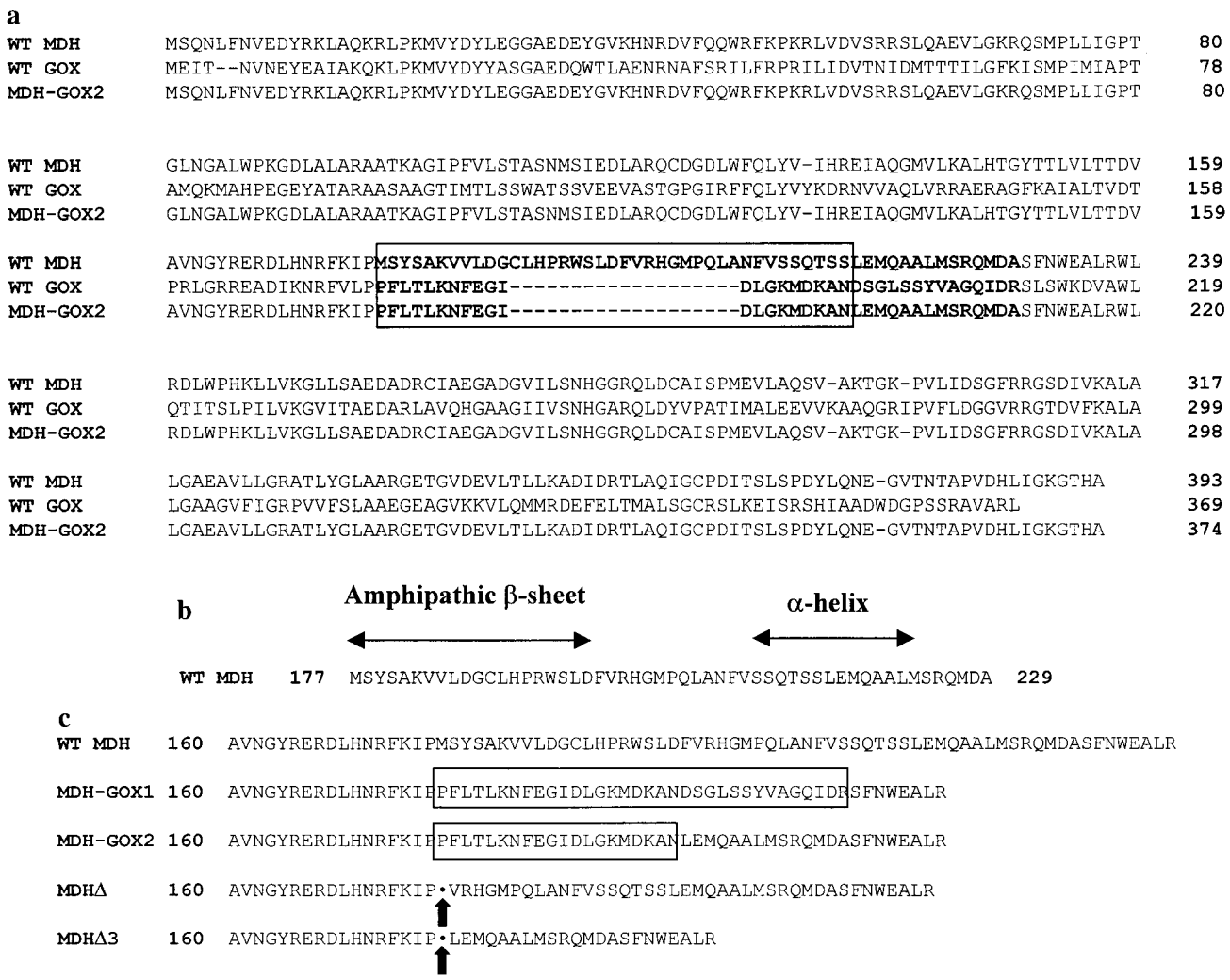

FIGURE 1: (a) Alignment of the sequences of (*S*)-mandelate dehydrogenase from *P. putida* (WT MDH), glycolate oxidase from spinach (WT GOX), and the MDH-GOX2 chimera. The 39-amino acid region enclosed in a box in WT MDH represents the internal sequences associated with membrane binding and was replaced with the corresponding segment from WT GOX in making the MDH-GOX2 chimera. The 53-amino acid segment of WT MDH shown in bold (including the boxed segment) was similarly replaced in making the MDH-GOX1 chimera. (b) Secondary structure predictions (*10*) for the 53-residue segment of WT MDH replaced in the MDH-GOX1 chimera and shown in bold in part a. (c) Partial sequences of MDH-GOX1, MDH-GOX2, and the Δ and Δ3 mutants of MDH. The arrows denote the positions at which residues were deleted from the sequence of MDH.

The members of the α-hydroxyacid oxidizing enzyme family also differ in their cellular localization. LMO is a soluble cytoplasmic enzyme; FCB2 is a soluble component of the mitochondrial intermembrane space, while GOX and LCHAO are localized within the peroxizome of the eukaryotic cells. MDH, on the other hand, is tightly bound to the bacterial membrane and can only be released through the action of detergents. A comparison of the sequences of several members of this family established that MDH differs substantially from the others over a 53-residue segment, from Met177 to Ala229 (*1*). A chimeric construct, named MDH-GOX2, in which 39 of these 53 residues in MDH were replaced with a corresponding 19-residue segment from GOX (Figure 1a), yielded an enzyme that was fully soluble and retained full wild-type activity for mandelate oxidation (*10*). This established that the membrane-binding portion of MDH was contained within this peptide segment, but that the segment did not effect mandelate oxidation. This segment, comprising residues 177−217 of MDH, aligns with a highly disordered 20-residue peptide segment in FCB2 and with a segment of similar length in GOX containing a disordered decapeptide according to their respective crystal structures (*6*, *7*). An earlier chimera, named MDH-GOX1, in which all 53 residues specific to MDH were replaced with the corresponding GOX segment, was also soluble but exhibited less than 1% of the wild-type catalytic activity for mandelate oxidation (*1*).

In this paper, we report, for the first time, the three-dimensional structure of a membrane-associated protein in which an intrachain integral membrane-binding segment is replaced with its soluble homologue to facilitate crystallization, but which still retains the catalytic activity of the wild type. A model is proposed for the association of MDH with the membrane.

EXPERIMENTAL PROCEDURES

Protein Purification. MDH-GOX2 was generated with a histidyl tag at its carboxy terminus and purified by affinity chromatography as described elsewhere (*10*).

Crystallization. Yellow crystals of MDH-GOX2 were obtained by the hanging-drop vapor-diffusion method at room

temperature. The optimized crystallization condition was as follows. A 3 μL drop of the protein solution (concentrated to 10−15 mg/mL) was mixed with 3 μL of the buffered precipitation mixture [0.2 M MES (pH 6.2), 0.75% ammonium sulfate, 10% ethylene glycol, and 20 μM FMN]; the reservoir solution contained 1 mL of 4.0 M NaCl. A precipitate formed first, followed by the slow appearance (3−7 days) of crystals from the precipitate. When the crystals were close to their maximal sizes but before the protein drop had completely dried out, they were transferred to a holding solution containing 0.3 M MES (pH 6.2), 1% ammonium sulfate, 20−25% ethylene glycol, and 30 μM FMN. The crystals could be stored for several weeks in this solution. The typical size of the crystals was 0.3 mm × 0.2 mm × 0.2 mm. Lower concentrations of NaCl in the reservoir resulted in smaller crystals. SDS−PAGE showed that the protein crystallized in its intact form.

X-ray Diffraction and Data Collection. X-ray diffraction data of crystals flash-frozen in the holding solution were collected using a Rigaku RU-200 rotating-anode X-ray source and an R-Axis IV Image plate area detector. The crystals diffracted to beyond 2.0 Å. A complete native data set to 2.0 Å resolution with an R_{merge} of 4.8% was initially obtained from a single crystal. Using the twinning test program obtained from the University of California at Los Angeles Twinning Center (*11*), it was determined that the crystals were perfectly twinned, as were most of the crystals that diffracted. To obtain an untwinned native data set, the twinned crystals were kept in the holding solution for 24 h. Then, under a microscope, the crystals were carefully cut into halves. Each half, with a size of 0.15 mm × 0.10 mm × 0.10 mm, was suitable for X-ray diffraction. A complete native data set to 2.15 Å was collected from one of these untwinned halves. The space group was determined to be *I*4 (tetragonal) with the following unit cell dimensions: $a = b = 99.6$ Å, and $c = 87.4$ Å (Table 1). The assumption of one polypeptide chain of MDH-GOX2 in the asymmetric unit leads to a Matthew's coefficient (*12*) of 2.6 Å^3/Da with a corresponding solvent content of 51.9%.

One uncut crystal was soaked with mercuric chloride for 1 h, and a complete data set to 3.0 Å resolution was collected. Fortunately, this crystal turned out to be untwinned. Both data sets were processed by the HKL package (*13*), leading to R_{merge} values of 0.092 and 0.140 for the native and derivative crystals, respectively. Both sets were nearly 100% complete (Table 1).

Structure Determination and Refinement. The structure of MDH-GOX2 was determined by the molecular replacement (MR) method with the program AMoRe (*14*). Since one monomer of MDH-GOX2 was expected in an asymmetric unit, a single subunit of glycolate oxidase [GOX, EC 1.1.3.1, PDB entry 1GOX (*7*)] was used as a polyalanine search model. One dominant solution with a correlation coefficient of 0.301 and an *R*-factor of 52.4% was obtained using data in the resolution range of 15−4 Å.

The MR solution of MDH-GOX2 was used as a starting model for refinement, which initially was carried out in the resolution range of 50−3 Å using the program CNS (*15*). For cross validation, 10% of the randomly selected data was set aside at the beginning of refinement by the calculation of R_{free} (*16*). All available data ($F > 0$) were used for refinement and for calculation of electron density maps. After initial rigid body refinement, the structure was further refined by variation of individual atomic positions with geometrical restraints (*17*). Manual rebuilding of the model was performed using Turbo-Frodo (*18*). As the refinement progressed, the amino acid sequence was changed to that of the MDH-GOX2 sequence and the *R* and R_{free} converged at 36.5 and 46.2%, respectively, and did not decrease further. Model bias from MR was then removed by single isomorphous replacement (SIR) by using phases obtained from the Hg derivative of MDH-GOX2. The binding sites for Hg were obtained using HEAVY (*19*). SIR phases calculated with HEAVY were combined with the phases of the refined model obtained by MR using SIGMAA (*20*). The resultant phases were improved using solvent flattening and histogram matching in the program DM (*21*). The resulting SIGMAA-weighted map was now greatly improved. The resolution range was gradually increased to 2.5 Å and then to 2.15 Å resolution by including individual atomic temperature factor refinement. Simulated annealing and positional and temperature factor refinement were alternated with manual model

Table 1: Data Collection, Structure Solution, and Refinement[a]

	native	Hg derivative
data collection		
wavelength (Å)	1.5418	1.5418
space group	*I*4	*I*4
unit cell dimensions (Å)	99.59	99.74
	99.59	99.74
	87.38	87.35
resolution limit (Å)	50−2.15	50−3
$I/\sigma(I)$	21.7 (6.3)	15.0 (6.5)
R_{merge}[b] (%)	9.2 (36.2)	14.0 (41.0)
completeness (%)	100 (100)	99.7 (100)
structure solution		
no. of sites		3
mean figure of merit		0.39 (0.33)
phasing power[c]		1.48
refinement		
resolution range (Å)	30−2.15	
R-factor[d] (%)	17.5	
R_{free}[e] (%)	21.2	
no. of reflections ($F > 0$)	22876	
model		
no. of amino acids[f]	349	
no. of water molecules	291	
no. of FMN	1	
no. of MES	1	
no. of sulfate	1	
residues in generously allowed regions	Asp188, Met192, Ser304, Leu189	
residues in disallowed regions	Glu32	
stereochemical ideality		
bonds (Å)	0.007	
angles (deg)	1.50	
dihedral angles (deg)	23.60	
improper angles (deg)	0.94	

[a] Values in parentheses refer to the highest-resolution shell. [b] $R_{merge}(I) = \sum|I_i - \langle I\rangle|/\sum I_i$, where I_i is the intensity of the *i*th observation, $\langle I\rangle$ is the mean intensity of the reflection, and the summation extends over all data. [c] Phasing power is the root-mean-square ($|F_H|/E$), where F_H is the calculated structure factor amplitude due to scattering by the heavy atom and *E* is the residual lack of closure error. [d] *R*-factor $= \sum||F_o| - |F_c||/\sum|F_o|$, where $|F_o|$ is observed structure factor amplitude, $|F_c|$ is calculated structure factor amplitude, and the summation extends over all data. [e] R_{free} is the *R*-factor obtained for a test set of reflections, consisting of a randomly selected 10% subset of the diffraction data, not used during refinement. [f] Twenty-seven atoms have zero occupancy.

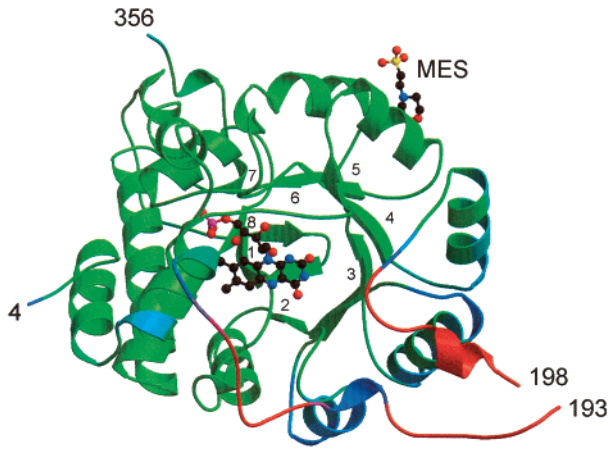

FIGURE 2: Ribbon diagram of the MDH-GOX2 structure. The ribbon is color-coded to indicate the average temperature factor of the various residues [$B \sim 20$ Å^2 (green), $B \sim 60$ Å^2 (red), and $B \sim 30$ and 45 Å^2 (blue and purple, respectively)]. The eight strands of the β-barrel are numbered, and the molecules of FMN and MES are indicated in atom colors [carbon (black), nitrogen (blue), oxygen (red), and phosphorus (magenta)]. This diagram was made using MOLSCRIPT (*40*) and RASTER3D (*41*).

building for several cycles. A total of 291 water molecules were added with the CNS program and carefully checked in the electron density. One molecule each of FMN, MES, and sulfate was also included in the model. The final model ($R = 17.5\%$; $R_{free} = 21.2\%$) includes 349 residues, one molecule each of FMN, MES, and sulfate, and 291 water molecules. The refined model has good geometry, according to the program PROCHECK (*22*). Eighty-seven percent of the amino acids are in the most favored region, and only one, Glu32, lies outside the allowed region. A summary of the crystallographic parameters, data processing, structure solution, and refinement statistics is given in Table 1.

RESULTS

Structure Analysis. The MDH-GOX2 mutant construct contains 380 amino acid residues and consists of residues 1−176 of MDH, residues 176−195 of GOX, and residues 216−399 of MDH, which includes a hexahistidyl tag at the C-terminus of the polypeptide chain (*10*). The refined molecular model of the MDH-GOX2 chimera consists of residues 4−193 and 198−356, with no electron density visible for residues 1−3, 194−197, and 357−380.

The temperature factors are generally low, with an average of ∼20−25 Å^2 over most of the MDH portion of the construct, residues 4−172 and 209−356 (Figure 2). The segment from residue 173 to 208 consists mostly of the GOX insert and has a substantially higher average B value, ∼55 Å^2, except for a short segment with a lower B value, residues 182−184, which forms main chain hydrogen bonding interactions with other parts of the structure. Within this mobile segment (residues 173−208), the main chain electron density is generally continuous at a contour level of 0.75−1.0σ (where σ is the mean electron density), except at residues 174, 176, and 200 where reduction of the contour level to 0.5σ is necessary for maintaining chain continuity. There was no electron density for side chains beyond the Cα or Cβ atoms for six residues (Arg70, Lys174, Ile175, Met192, Asp193, and Arg206), and the occupancies for these atoms (27 in total) have been set to zero.

Molecular Structure. MDH-GOX2 crystallizes in an *I*-centered tetragonal unit cell containing one molecule in the asymmetric unit and eight molecules in the unit cell. Within the crystals, quartets of MDH-GOX2 monomers pack together about the crystallographic 4-fold axes to form tightly packed tetramers. The solvent inaccessible interface between monomers within each tetramer has a surface area of ∼1900 Å^2 per monomer. The surface area buried by intermolecular contacts between tetramers in the crystal that are related by unit cell translations along *a* or *b* and by body centering is considerably smaller, ∼350 and ∼675 Å^2 per monomer, respectively. The latter contacts are mediated largely by molecules of bound MES through direct and water-mediated electrostatic interactions.

As predicted on the basis of sequence homology with other members of the α-hydroxyacid oxidizing enzyme family (*3*), MDH-GOX2 is folded as a $\beta_8\alpha_8$ TIM barrel with the FMN prosthetic group located at the C-terminal end of the β-barrel (Figure 2). It is positioned close to the barrel axis with the *re* face of the flavin ring lying on top of strand β-1 and its N-5 atom accepting a hydrogen bond from the peptide amide of Gly81; the phosphate group of FMN is inserted between the ends of strands β-7 and β-8. Above the flavin ring, opposite its *si* face, are the side chains of seven residues, Tyr26, Tyr131, Asp158, Arg165, Lys231 (Lys250 in wild-type MDH), His255 (His274 in wild-type MDH), and Arg258 (Arg277 in wild-type MDH) (Figure 3) that are highly conserved in this family of proteins and are believed to be important in catalysis during the reductive half-reaction. During refinement of the structure, the $F_o - F_c$ electron density was found to contain a piece of strong electron density ∼4 Å above the flavin ring and greater than 8σ in magnitude. The peak is roughly spherical in shape and corresponds in position approximately to the carboxylate group of a pyruvate anion, which had been modeled into the FCB2 structure (*6*). The center of the peak is within ∼3−4 Å of two arginine side chains, a histidine side chain, and a water molecule. The water is part of a chain of three water molecules that connects the hydroxyl groups of Tyr26 and Tyr131. The peak has been modeled as a sulfate anion since that was the only small anion present in the crystallization drop to any appreciable extent.

Comparison to GOX and FCB2. The conformation of MDH-GOX2 is closely similar to that of GOX and of FCB2, in both ternary and quaternary structure. When monomers of MDH-GOX2 and GOX are aligned, the root-mean-square (rms) deviation of Cα atoms is 1.00 Å for 305 equivalent residues (Figure 4). This similarity extends to their quaternary structures as well. When dimers (half-tetramers) of the two molecules are superimposed, the rms deviation between equivalent Cα atoms is 1.10 Å for 612 equivalent residues. However, this similarity in quaternary structure does not extend beyond the tetramer. MDH-GOX2 tetramers pack into the crystal in a checkerboard fashion, consistent with its *I*4 space group symmetry. GOX forms octamers with molecular 422 symmetry as dictated by its space group symmetry, *I*422, in which one octamer is located at the origin of the unit cell. Interestingly, MDH-GOX2 behaves in solution like a larger aggregate, most likely an octamer (unpublished results), but since such a structure is inconsistent with the space group symmetry, the crystal structure gives no indication of how this larger oligomer is organized.

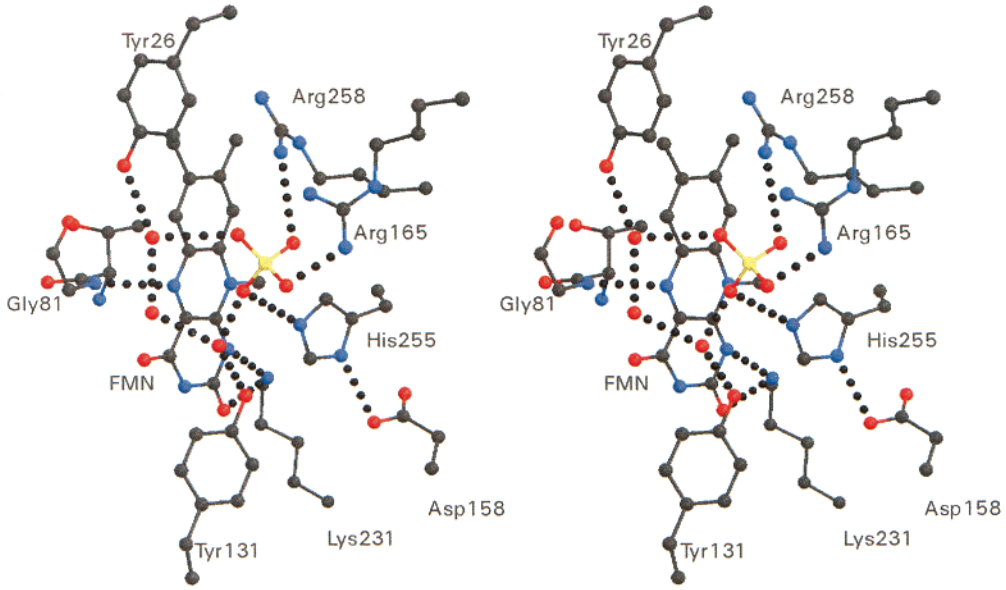

FIGURE 3: Active site of MDH showing the flavin and seven active site side chains (Tyr26, Tyr131, Asp158, Arg165, Lys231, His255, and Arg258) that are conserved among the α-hydroxyacid oxidizing enzymes. For the latter three residues, the residues in wtMDH are Lys250, His274, and Arg277, respectively. The Gly81 amide to flavin N-5 hydrogen bond is also shown. A chemical group modeled as a sulfate anion, above the flavin ring, as well as three water molecules linking some of the active site residues are shown using the atom colors described in the legend of Figure 2, with sulfur in yellow. This diagram was made using MOLSCRIPT (*40*).

The dimer interface of both MDH-GOX2 and GOX contains both hydrophobic and hydrophilic interactions. The MDH-GOX2 interface is held together by 17 hydrogen bonds (four main chain (MC)−MC, six MC−side chain (SC), and seven SC−SC), while the GOX interface is bridged by 21 hydrogen bonds (four MC−MC, three MC−SC, and 14 SC−SC). The positions of two of the MC−MC hydrogen bonds (F49α−C262β and V57α−A210β of MDH-GOX2 and F47α−Y261β and V55α−R209β of GOX, where α and β refer to different subunits) and two of the MC−SC hydrogen bonds (F6α−Y164β and R53α−D238β of MDH-GOX2 and T4α−R163β and I51α−D237β of GOX) are conserved in the two structures. The SC−SC hydrogen bonding interactions are generally not conserved, except for a set of three interactions involving four conserved residues (N7α−E166β, R289α−E166β, and R289α−D33β of MDH-GOX2 and N5α−E165β, R290α−E165β, and R290α−D31β of GOX).

Comparing the subunits of MDH-GOX2 with those of FCB2 indicates an rms deviation of 0.92 Å for 294 equivalent Cα atoms while superimposition of the dimers shows rms deviation for equivalent residues of 1.03 Å for 575 Cα atoms. Thus, the structural homology of MDH-GOX2 appears to be the same with both FCB2 and GOX. Six of the seven conserved dimer interactions between MDH-GOX2 and GOX are also retained in the FCB2 interface. Interestingly, the structural conservation among MDH-GOX2, GOX, and FCB2 extends to the single residue of MDH-GOX2, Glu32, which lies outside the allowed region of the Ramachandran diagram and is part of a type II′ turn which normally has glycine at this position. In GOX and FCB2, the corresponding residues are Glu30 and Asn149, respectively, and are also in the same disallowed region, with average dihedral angles ϕ of 42° and ψ of −113° for the three proteins. This residue is located in the tetramer interface within each structure, adjacent to one of the conserved SC−SC salt bridges (R289α−D33β in MDH-GOX2) and probably plays a role in tetramer stabilization.

In MDH-GOX2, the segment shown to be responsible for the binding of native MDH to the membrane, residues 177−215, has been replaced with residues 176−195 of GOX and consequently is 19 residues shorter. In the GOX crystal structure, the last seven of these residues (residues 189−195) are disordered, along with the following two residues, leaving a 12 Å spatial gap between the ordered ends (*7*). In MDH-GOX2, only the last three residues of this segment, and the first residue of the remaining MDH segment, are disordered, leaving a 5 Å spatial gap. Residues 177−189 are similar in conformation to the corresponding segment of GOX, following a closely similar path up to position 185 (rmsd = 1.3 Å) and a more divergent path to residue 189 (rmsd = 4.8 Å) (Figure 4). From positions 198−206, which revert to MDH in sequence, the polypeptide chain is largely α-helical, as predicted from the sequence (*10*) (Figure 1b). However, the helix points in a direction different (by ∼100°) from that of the corresponding segment of GOX (residues 198−205, also α-helical) and extends into solution (Figure 4). Thus, the conformation of the GOX insert appears to be largely dictated by its GOX amino acid sequence, while that of the following MDH segment may reflect the conformation dictated by its own sequence, although possibly perturbed by the absence of the membrane-binding portion of the native MDH molecule.

In FCB2, there is a highly disordered, protease-sensitive peptide segment extending from approximately position 300 to 317 (*6*), which corresponds roughly to the membrane-binding segment of MDH and to the GOX insert in MDH-GOX2 (*8*). However, the short peptide segments visible at either end (residues 295−299 and 317−322) extend away from the remainder of the molecule in a direction different from that in either MDH-GOX2 or GOX. Kinetic studies indicate that this loop does affect the catalytic properties of FCB2 (*4*). On the other hand, a portion of the cytochrome domain of FCB2 (positions 61−77) does correspond in position to the C-terminal part of the GOX insert engineered

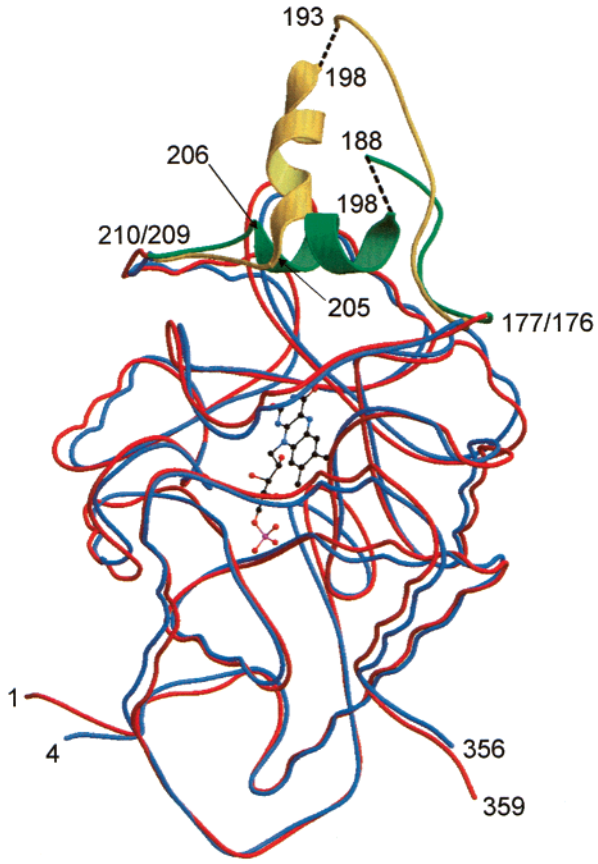

FIGURE 4: Structural comparison of MDH-GOX2 with GOX. The highly conserved segments of MDH-GOX2 (residues 4−176 and 211−356) and GOX (residues 1−175 and 210−359) are shown in blue and red, respectively. The poorly conserved segments of MDH-GOX2 (residues 177−210) and GOX (residues 176−209) are in yellow and green, respectively. The polypeptide chains are shown as coils except for the helical segments of MDH-GOX2 (residues 198−206) and GOX (residues 198−205) within the poorly conserved segments which are shown as helical ribbons. The disordered segments in MDH-GOX2 (residues 194−197) and GOX (residues 189−197) are shown as dashed lines. This diagram was made using MOLSCRIPT (*40*) and RASTER3D (*41*).

into MDH-GOX2 (positions 177−189). In FCB2, the cytochrome domain serves to cover the top of the $\beta_8\alpha_8$ barrel and limit access of the flavin ring to bulk solvent.

Flavin Conformation. The conformation and flavin orientation of the FMN in MDH-GOX2, with its *re* face in contact with strand β-1 and its N-5 atom accepting a hydrogen bond from the amide of Gly81, are closely similar to those in FCB2. This orientation differs significantly from that in the native GOX structure, where the flavin ring is displaced and unable to make contact with the first β-strand of the barrel (Figure 5). This displacement arises from differences in the torsion angles about the C-2*−C-1* and C-1*−N-10 bonds of FMN that result in an ∼20° tilt of the flavin ring which effectively pivots about the C-8−C-9 bond. The largest displacements are at O-4 (∼2.5 Å) and O-2 (∼2 Å). The positions of the ribityl phosphate chains are virtually identical, however, in all three structures. In GOX, the side chain and main chain atoms adjacent to the active site also move to accommodate the shift of the flavin ring, and the same hydrogen bonding pattern is generally maintained within the active site. However, a water molecule in GOX fills a void left in the structure by displacement of the flavin ring and bridges the main chain carbonyl of Thr78 and the hydroxyl of Ser106, while O-4 of the flavin forms a hydrogen bond to Tyr129. In MDH-GOX2, the equivalent Ser108 forms a hydrogen bond to the flavin O-4 and Tyr131 is hydrogen bonded to the side chain of His255 (Figure 5). Comparison of the backbone ϕ and ψ residues, respectively, of residues Thr80 and Thr78 in MDH-GOX2 with those of Gly81 and Ala79 in GOX shows that they differ by ∼120° and ∼100°, respectively, leading to breaking of the N-5−carbonyl hydrogen bond in MDH-GOX2 and formation of the hydrogen bonds to the water molecule in GOX. These structural differences are nearly identical to those observed previously from comparison of FCB2 and GOX (*8*).

DISCUSSION

Structural Conservation within the α*-Hydroxyacid Oxidizing Enzymes.* The sequence conservation within this family of FMN-dependent enzymes was described previously (*3*, *8*) and has led to predictions of conservation of the catalytic mechanism in the reductive half-reaction. This conservation has been borne out by mutagenic studies of individual enzyme family members (*23*), including MDH (*24*, *25*). The present structure is the third for this family to be determined and confirms the predicted structural conservation among these family members (*1*). This conservation appears to be maintained despite the clear differences between the oxidative half-reactions. FCB2 is a flavodehydrogenase, in which single electrons are transferred to cytochrome electron acceptors, while GOX is a flavoprotein oxidase, in which molecular oxygen receives a pair of electrons with generation of hydrogen peroxide. The electron acceptor for MDH is not known, but is likely to be a quinone component of the bacterial electron transport chain, in view of its localization in the cytoplasmic membrane.

It is intriguing that this structural conservation among these representatives of three distinct subfamilies extends in part to their quaternary structures, as all three enzymes form very stable tetramers with circular 4-fold symmetry, although GOX forms also a weak octamer (*7*) and MDH-GOX2 appears to form higher oligomers in solution, possibly octamers. The subunits of the tetramers of all three enzymes interlock with their partner subunits by utilizing the same elements of tertiary structure and involve highly similar hydrogen bonding and van der Waals interactions. The large areas of their subunit interfaces are comparable in magnitude, involve similar distributions of hydrophobic and hydrophilic side chains, and even contain a conserved Ramachandran outlier, Glu32.

Enzyme Activities of MDH-GOX Chimeric Constructs. The portion of MDH-GOX2 following the membrane-binding segment, residues 198−206, adopts an α-helical conformation (Figure 4) as predicted (*10*) (Figure 1b). In an earlier mutagenic study (*1*), a 53-residue segment of MDH (residues 177−229) was replaced with a 34-residue segment of GOX (residues 176−209). This mutation yielded a soluble enzyme, MDH-GOX1 (Figure 1c), but with greatly reduced catalytic activity. It is not clear from the present structure how the absence of the segment of residues 216−229 originally present in MDH (and now numbered 197−210 in the MDH-GOX2 structure) would compromise the enzymatic activity since that segment is directed away from the active site

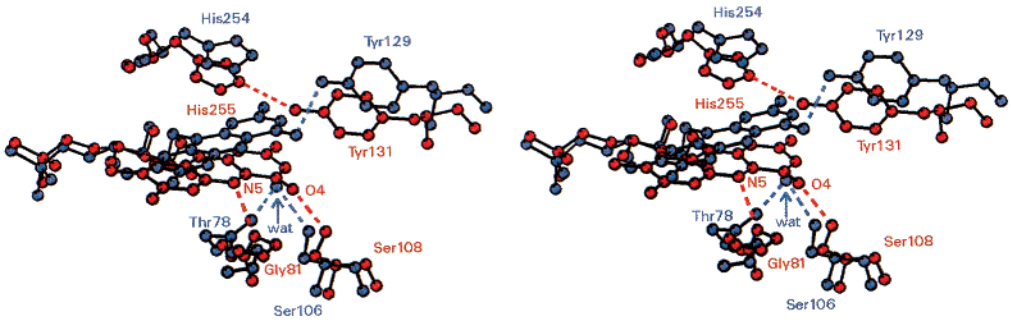

FIGURE 5: Conformation of FMN in MDH-GOX2 and in GOX. MDH-GOX2 is shown in a red ball-and-stick representation, and GOX is shown in blue. The residue and atom labeling and hydrogen bonding follow the same convention. Three pairs of side chains in the two structures (His254 and His255, Tyr129 and Tyr131, and Ser106 and Ser108) and the main chain atoms of one pair of residues (Thr78 and Gly81) are involved in altered hydrogen bonding arrangements with the flavin ring and with each other in GOX and MDH-GOX2, respectively. The water molecule in GOX that displaces the flavin ring of MDH-GOX2 is also shown. This diagram was made using MOLSCRIPT (*40*).

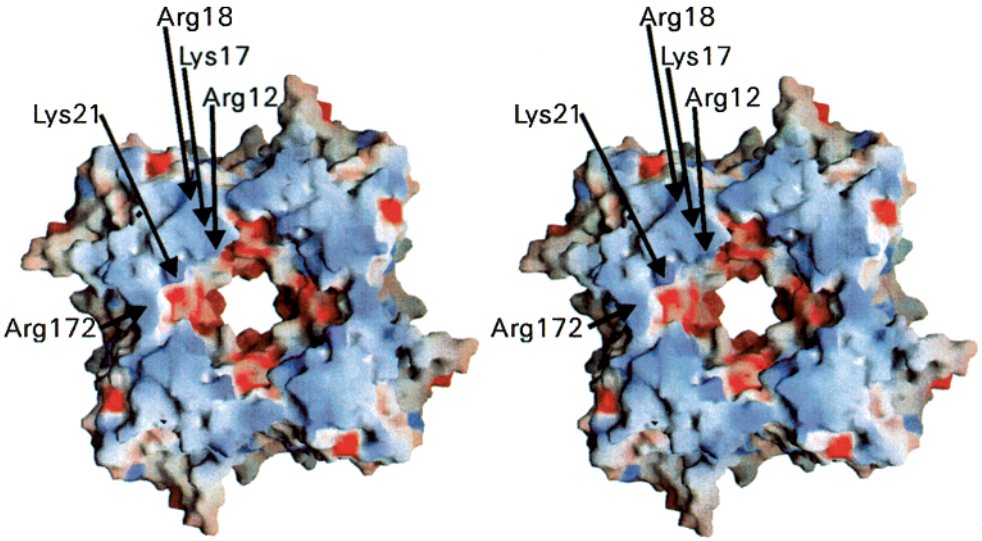

FIGURE 6: Electrostatic surface potential of the MDH-GOX2 tetramer calculated with the GOX insert (residues 177−193) omitted. Positive potential is in blue, and negative potential is in red. Five basic side chains in one of the four monomers on the visible surface that are proposed to interact with the phospholipid membrane surface are indicated. This diagram was produced using GRASP (*14*).

region and toward the exterior of the MDH-GOX2 structure (Figure 4). However, in the MDH-GOX1 molecule, the corresponding helical segment introduced from GOX (residues 198−205) might readily adopt the same configuration as it does in native GOX, causing the intervening segment of the GOX sequence [residues 189−197, which are disordered in the native GOX crystal structure (*7*)] to interfere with the normal catalytic function of MDH. Since only four residues in the central part of MDH-GOX2 are disordered, it is less likely that this segment will perturb the active site.

Implications for Membrane Interactions. To obtain maximum catalytic efficiency during turnover, the MDH tetramer should be oriented with its 4-fold axis perpendicular to the membrane surface so that all four of its subunits have equal access to the bacterial membrane. The MDH-GOX2 tetramer, when the GOX insert is omitted, has a net charge of zero, assuming Glu and Asp each have a negative charge, Lys and Arg each have a positive charge, and all the other residues are uncharged (*14*). The electric dipole moment computed on this basis has a magnitude of ∼3000 D. While the face in the opposite direction from the dipole vector is distinctly electronegative, the external face of the tetramer in the positive dipole direction has a distinctly electropositive potential surface (*26*) (Figure 6). This electropositive surface forms a circular ridge which projects beyond the protein surface by ∼4 Å. It is most likely to interact with the negatively charged phospholipid headgroups of the bacterial membrane and could provide a major contact surface with the membrane. Although this electrostatic interaction would help stabilize binding to the membrane, it is not sufficient to do so since the MDH-GOX2 mutant is soluble. Likewise, two deletions mutants of MDH, Δ and Δ3 (Figure 1c), which lack part or all of the membrane-binding peptide, are also soluble, although the Δ mutant did display aggregation behavior (*10*).

Pro176, the residue just preceding the membrane-binding segment, is located ∼4 Å from the electropositive surface of the tetramer, and is situated so that the N-terminal end of the following residue, Met177, could insert directly into the membrane. The predicted structure for the first 20 residues of this membrane-binding segment is that of an amphipathic β-sheet (*10*) (Figure 1b), and the remaining 20 include nine hydrophobic residues and one charged residue. Therefore, this segment is likely to be tightly associated with the membrane and could provide a channel between the hydrophobic membrane interior and the enzyme active site for translocation of the lipophilic substrate. It is unlikely that the entire 39-residue membrane-binding segment of MDH is associated with the membrane since its C-terminal end must connect to Glu217 at the N-terminus of the short helix,

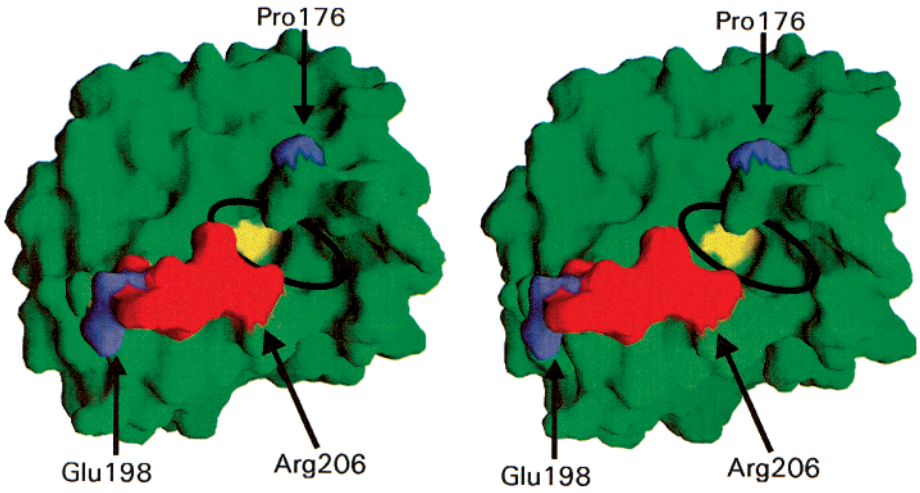

FIGURE 7: GRASP (*14*) rendition of the molecular surface of MDH-GOX2, with the GOX insert omitted. The two residues of MDH-GOX2 adjacent to the membrane-binding segment that is replaced by the GOX segment in the chimera, Pro176 and Glu198, are indicated in blue. The peptide segment of Met199−Arg206 is indicated in red. The visible surface of the flavin ring is shown in yellow, and the mouth of a funnel leading to it is depicted as a black ellipse.

some 20 Å from the putative membrane surface. The Δ3 deletion mutant [lacking the 39-residue membrane-binding segment (*10*), Figure 1c], in which Pro176 is joined directly to Leu216, displays poor enzymatic activity, indicating that drastic movement of the helix is deleterious. Therefore, the last six residues of the segment, which are neutral hydrophilic, could serve as a link back to the remainder of the MDH molecule.

Thus, our present model for the binding and interaction of MDH with the membrane surface consists of two parts. One is an association partially stabilized by electrostatic interactions between the electropositive surface of the MDH tetramer and the electronegative membrane surface. The second consists of partial membrane insertion of the 39-residue peptide segment that is necessary for membrane binding. This segment would provide the improved stabilization needed for binding, provide an access channel to the active site of the physiological oxidant of FMN, and traverse the protein surface to connect to Glu217, 20 Å above the putative membrane surface.

Other Membrane-Associated Proteins. MDH appears to belong to the monotopic class of integral membrane proteins (*27*) that are inserted into only one side of the phospholipid bilayer rather than spanning the entire membrane. Other members of this class whose structures are known are prostaglandin H_2 synthase (PHS) (*28*, *29*), squaline-hopene cyclase (SHC) (*30*), and the C-2 membrane-binding domains of coagulation factors Va (*31*) and Viiia (*32*). SHC and PHS are dimeric proteins that contain nonpolar membrane-binding surface regions surrounding the entrance channels leading to the enzyme active site. Furthermore, the dimers of both enzymes are oriented so that the putative membrane binding surfaces are coplanar, permitting both monomers to bind to the membrane at once. However, there appears to be no electrostatic interaction of SHC or PHS with the membrane. The two C-2 coagulation factor domains appear to interact with the membrane through several hydrophobic residues located on short loops at one end of the molecule and to be attracted to the negatively charged phospholipid headgroups of the membrane through electrostatic interactions with lysine and arginine residues. MDH appears to combine features of both types of protein, having, like the C-2 domains, both hydrophobic insertion and electrostatic stabilization of membrane binding and, like the PHS and SHC, coplanar membrane-binding surfaces and channels leading to the active site.

D-Lactate dehydrogenase (DLDH) from *Escherichia coli* is a peripheral membrane flavoprotein (*33*) having a large electropositive surface but apparently no membrane penetration, since the enzyme can be released under conditions of high salt. However, it also contains a disordered segment of nearly 50 residues within the membrane-binding domain. This segment is not believed to penetrate the membrane, but to provide additional electrostatic attraction through the interaction of its basic residues with the electronegative membrane surface (*33*). Thus, DLDH differs in a fundamental way from the monotopic integral membrane proteins represented by MDH, PHS, SHC, and the C-2 coagulation factor domains discussed above.

The number of water molecules present per subunit in the hydration shell [within 3.6 Å of the protein surface (*34*, *35*)] of MDH-GOX2, GOX, DLDH, and C-2 factor VIIIa are 269, 243, 234, and 202, respectively. In GOX, DLDH, and C-2 factor VIIIa, the water molecules cover the entire exposed surface of the molecules uniformly with no discernible pattern, although in DLDH the coverage is sparse. In MDH-GOX2, however, the water molecules are segregated over the surface of the tetramer, being absent from the concentric ring of elevated positively charged residues on the electropositive surface and uniformly distributed elsewhere. This may allow the positively charged residues to interact freely with the electronegative surface of the phospholipids.

Substrate Access to the Active Site. MDH reacts with two types of substrates, a reductant, mandelate, and an oxidant, probably a quinone. These two substrates are localized in different compartments of the bacterial cell, the reductant residing in the aqueous cytoplasmic phase and the oxidant residing in the membrane phase. There is a funnel-shaped opening located between the positions of Pro176 and Arg206 (Figure 7) which leads to the solvent-accessible flavin ring in the active site. The mouth of the funnel is elliptical in shape, with its long axis oriented roughly perpendicular to

the 4-fold axis of the tetramer. The 39-residue segment of MDH replaced with GOX in MDH-GOX2 provides, according to our model, a channel through which the quinone can reach the active site through one side of the funnel, leaving room on the other side of the funnel for substrate access from the cytoplasm. The lack of a structure for this segment prevents further speculation about its role in providing substrate access from the membrane phase.

Oxidative Half-Reaction. As described earlier, GOX has a binding site for a water molecule on the *re* face of the flavin ring that is present because the flavin ring is displaced by a tilt of ~20° with respect to its orientation in FCB2 and MDH-GOX2 (Figure 4). It has been proposed that this water position is the binding site for dioxygen when the flavin becomes reduced and that dioxygen can then reoxidize the flavin through formation of a transient covalent peroxo intermediate (*8*). If this alternate orientation of the flavin were energetically disfavored in FCB2 and MDH-GOX2 because of steric interactions, that could account for the slow rate of reoxidation of the reduced flavin by dioxygen in the latter two enzymes. The plasticity of the GOX active site and its flavin orientation have been demonstrated in two inhibitor-bound forms of GOX in which the flavin conformation matches that in FCB2 and MDH-GOX2 (*36*). In one of these structures (3-decyl-2,5-dioxo-4-hydroxy-3-pyrroline), the flavin N-5 to Thr78 carbonyl hydrogen bond is also restored, while in the other [4-carboxy-5-(1-pentyl)hexasulfanyl-1,2,3-triazole], it is not because of differences in the peptide geometry of residues 77 and 78. In none of the known recombinant (*37*) or mutant (*38*, *39*) FCB2 or MDH-GOX2 structures is reorientation of the flavin ring observed; examination of the MDH-GOX2 or FCB2 structures has so far not indicated the potential source of any flavin rigidity. Clearly, further investigation of the regulation of the oxygen reactivity of the flavin ring is needed for this family of flavoenzyme oxidases and dehydrogenases.

ACKNOWLEDGMENT

We thank Dr. Graham Bentley of the Institut Pasteur (Paris, France) for advice in MR and SIR phase combination. We are grateful to Dr. Tongqing Zhou for assistance in the early part of this work.

REFERENCES

1. Mitra, B., Gerlt, J. A., Babbitt, P. C., Koo, C. W., Kenyon, G. L., Joseph, D., and Petsko, G. A. (1993) *Biochemistry 32*, 12959−12967.
2. Maeda-Yorita, K., Aki, K., Sagai, H., Misaki, H., and Massey, V. (1995) *Biochimie 77*, 631−642.
3. Diep Le, K. H., and Lederer, F. (1991) *J. Biol. Chem. 266*, 20877−20881.
4. Lederer, F. (1991) Flavocytochrome b_2, in *Chemistry and Biochemistry of the Flavoenzymes* (Muller, F., Ed.) Vol. 2, pp 153−242, CRC Press, Boca Raton, FL.
5. Ghisla, S., and Massey, V. (1991) L-Lactate Oxidase, in *Chemistry and Biochemistry of the Flavoenzymes* (Muller, F., Ed.) Vol. 2, pp 243−289, CRC Press, Boca Raton, FL.
6. Xia, Z.-x., and Mathews, F. S. (1990) *J. Mol. Biol. 212*, 837−863.
7. Lindqvist, Y. (1989) *J. Mol. Biol. 209*, 151−166.
8. Lindqvist, Y., Branden, C. I., Mathews, F. S., and Lederer, F. (1991) *J. Biol. Chem. 266*, 3198−3207.
9. Stenberg, K., Clausen, T., Lindqvist, Y., and Macheroux, P. (1995) *Eur. J. Biochem. 228*, 408−416.
10. Xu, Y., and Mitra, B. (1999) *Biochemistry 38*, 12367−12376.
11. Yeates, T. O. (1997) *Methods Enzymol. 276*, 344−358.
12. Matthews, B. W. (1968) *J. Mol. Biol. 33*, 491−497.
13. Otwinowski, Z., and Minor, W. (1997) *Methods Enzymol. 276*, 307−326.
14. Navaza, J. (1994) *Acta Crystallogr. A50*, 157−163.
15. Brünger, A. T., Adams, P. D., Clore, G. M., DeLano, W. L., Gros, P., Grosse-Kunstleve, R. W., Jiang, J.-S., Kuszewski, J., Nilges, M., Pannu, N. S., Read, R. J., Rice, L. M., Simonson, T., and Warren, G. L. (1998) *Acta Crystallogr. D54*, 905−921.
16. Brünger, A. T. (1992) *Nature 355*, 472−475.
17. Engh, R. A., and Huber, R. (1991) *Acta Crystallogr. A47*, 472−475.
18. Roussel, A., and Cambillau, C. (1991) in *Silicon Graphics Geometry Partners Directory 86*, Silicon Graphics, Mountain View, CA.
19. Terwilliger, T. C., and Berendzen, J. (1999) *Acta Crystallogr. D55*, 849−861.
20. Read, R. J. (1986) *Acta Crystallogr. A42*, 140−149.
21. Cowtan, K., and Main, P. (1998) *Acta Crystallogr. D54*, 487−493.
22. Morris, A. L., MacArthur, M. W., Hutchinson, E. G., and Thornton, J. M. (1992) *Proteins 12*, 345−364.
23. Lederer, F., Belmouden, A., and Gondry, M. (1986) *Biochem. Soc. Trans. 24*, 77−83.
24. Lehoux, I. E., and Mitra, B. (1999) *Biochemistry 38*, 9948−9955.
25. Lehoux, I. E., and Mitra, B. (2000) *Biochemistry 39*, 10055−10065.
26. Nicholls, A., Sharp, K. A., and Honig, B. (1991) *Proteins 11*, 281−296.
27. Blobel, G. (1980) *Proc. Natl. Acad. Sci. U.S.A. 77*, 496−500.
28. Picot, D., Loll, P. J., and Garavito, R. M. (1994) *Nature 367*, 243−249.
29. Kurumbail, R. G., Stevens, A. M., Gierse, J. K., McDonald, J. J., Stegeman, R. A., Pak, J. Y., Gildehaus, D., Miyashiro, J. M., Penning, T. D., Seibert, K., Isakson, P. C., and Stallings, W. C. (1996) *Nature 384*, 644−648.
30. Wendt, K. U., Lenhart, A., and Schulz, G. E. (1999) *J. Mol. Biol. 286*, 175−187.
31. Macedo-Ribeiro, S., Bode, W., Huber, R., Quinn-Allen, M. A., Kim, S. W., Ortel, T. L., Bourenkov, G. P., Bartunik, H. D., Stubbs, M. T., Kane, W. H., and Fuentes-Prior, P. (1999) *Nature 402*, 434−439.
32. Pratt, K. P., Shen, B. W., Takeshima, K., Davie, E. W., Fujikawa, K., and Stoddard, B. L. (1999) *Nature 402*, 439−442.
33. Dym, O., Pratt, E. A., Ho, C., and Eisenberg, D. (2000) *Proc. Natl. Acad. Sci. U.S.A. 97*, 9413−9418.
34. Kodandapani, R., Suresh, C. G., and Vijayan, M. (1990) *J. Biol. Chem. 265*, 16126−16131.
35. Sukumar, N., Biswal, B. K., and Vijayan, M. (1999) *Acta Crystallogr. D54*, 934−937.
36. Stenberg, K., and Lindqvist, Y. (1997) *Protein Sci. 6*, 1009−1015.
37. Tegoni, M., and Cambillau, C. (1994) *Protein Sci. 3*, 303−313.
38. Tegoni, M., Begotti, S., and Cambillau, C. (1995) *Biochemistry 34*, 9840−9850.
39. Mowat, C. G., Beaudoin, I., Durley, R. C., Barton, J. D., Pike, A. D., Chen, Z. W., Reid, G. A., Chapman, S. K., Mathews, F. S., and Lederer, F. (2000) *Biochemistry 39*, 3266−3275.
40. Kraulis, P. J. (1991) *J. Appl. Crystallogr. 24*, 946−950.
41. Merritt, E. A., and Bacon, D. J. (1997) *Methods Enzymol. 277*, 505−524.

BI010938K